ELSEVIER

Journal of Nuclear Materials 277 (2000) 333–338

journal of nuclear materials

www.elsevier.nl/locate/jnucmat

Influence of technetium on the microstructure of a stainless steel–zirconium alloy

D.D. Keiser Jr.[a], D.P. Abraham[b,*], J.W. Richardson Jr.[b]

[a] *Argonne National Laboratory-West, P.O. Box 2528, Idaho Falls, ID 83403, USA*
[b] *Argonne National Laboratory, 9700 S. Cass Avenue, Argonne, IL 60439-4837, USA*

Received 13 April 1999; accepted 21 June 1999

Abstract

Stainless steel–zirconium alloys are being developed for the disposal of metallic waste generated during the electrometallurgical treatment of spent Experimental Breeder Reactor (EBR-II) fuel. The metallic waste contains the fission product technetium, which must be incorporated into a stable waste form matrix to prevent its release into the environment. The baseline waste form for metallic waste from EBR-II fuels is a stainless steel–15 wt% zirconium (SS–15Zr) alloy. The microstructure of SS–15Zr alloys containing 2 wt% technetium was characterized using a combination of microscopy, spectroscopy, diffraction, and chemical analysis techniques. Peaks corresponding to the iron solid solutions ferrite and austenite, $ZrFe_2$-type Laves polytypes C36 and C15, and an $Fe_{23}Zr_6$-type intermetallic were identified in diffraction patterns of the alloy. Discrete technetium-rich phases were not observed either in diffraction patterns or in the microstructure; the element partitioned into various phases of the SS–15Zr alloy. Technetium favors ferrite and austenite over the Zr-based intermetallics. The lattice parameters of the Zr-based intermetallics are smaller than those in an alloy without technetium, which appears to substitute at the zirconium sites of the intermetallic lattice.

PACS: 61.12.Yp; 61.16.Bg; 28.41.Kw

1. Introduction

Technetium is a metallic element in group VIIb of the periodic table. It is artificially produced by fission of U-235 during nuclear reactor operation [1]. Technetium is one of many fission product elements present in the Experimental Breeder Reactor-II (EBR-II) spent nuclear fuel being treated by an electrometallurgical process at Argonne National Laboratory (ANL). In this treatment process, chopped fuel elements are loaded into the anode baskets of an electrorefiner. The uranium in the spent fuel is electrolytically dissolved and deposited on a steel cathode. The remnants in the anode baskets, which include cladding hulls, fuel components, actinides, and fission products such as Tc, are consolidated by melting and cast into an alloy ingot referred to as the metal waste form (MWF) [2]. The waste form contains the radioactive isotopes for eventual disposal in a geologic repository. The baseline waste form selected for stainless steel-clad fuels (such as the EBR-II fuels) is stainless steel – 15 wt% zirconium (SS–15Zr) alloy [3].

Among the many radionuclides present in waste forms Tc-99 is particularly important because of its relative abundance and long half-life (2.1×10^5 yr) [4,5]. It is highly soluble in geologic groundwaters as the pertechnetate anion TcO_4^- and can diffuse readily through geologic systems. Thus, incorporation of Tc-99 into a stable waste form matrix is necessary to prevent its release into the biosphere [6,7]. This article discusses the incorporation of Tc in the phases of a SS-15Zr alloy. An understanding of technetium distribution in SS–15Zr alloy phases is needed to predict the leach behavior of the element in corrosive environments.

* Corresponding author. Tel.: +1-630 252 4332; fax: +1-630 972 4406.
E-mail address: abraham@cmt.anl.gov (D.P. Abraham).

0022-3115/00/$ - see front matter
PII: S0022-3115(99)00158-0

In our laboratory, stainless steel – 15 wt% zirconium – 2 wt% technetium (SS–15Zr–2Tc) alloys were prepared in a resistance-heated furnace. The alloys were characterized using a combination of microscopy, spectroscopy, diffraction, and chemical analysis. The influence of technetium on alloy microstructure was determined by comparing the results with those from Tc-free SS–15Zr alloys. Results of corrosion studies on Tc-containing SS–15Zr alloys will be presented in future articles.

2. Experimental details

The technetium metal used in our alloys was prepared by reducing ammonium pertechnetate under a H_2 atmosphere at 900°C; the reduced metal was then stored under an inert atmosphere. The purity of the metal was determined by X-ray diffraction and beta spectroscopy, which indicated a ~90% reduction of the ammonium pertechnetate.

The alloy mixture containing type 316 stainless steel, zirconium, and technetium was contained in a yttrium oxide crucible (17 mm diameter and 49 mm tall), heated to 1600°C under an argon atmosphere, and cooled slowly (<10°C/min) to room temperature. The resulting SS–15Zr–2Tc alloy ingots weighed ~10 g. Technetium volatilization during high-temperature processing is a known problem [8,9]. Metallic Tc has a melting point of 2172°C, but it forms the stable oxide Tc_2O_7, which boils at 310.6°C. The Tc content of our alloy samples was measured by chemical analysis and is listed in Table 1. Alloy samples were dissolved in an aqua regia – 2 vol.% hydrofluoric acid solution, and Tc content was determined by liquid scintillation spectroscopy. The amounts of other elements in the alloy were determined by inductively coupled plasma-optical emission spectroscopy, performed with an ARL 3580B spectrometer interfaced with a shielded glove box. Table 1 shows that most of the Tc was incorporated within the alloy samples.

Time-of-flight (TOF) neutron diffraction data were collected from an alloy sample on the General Purpose Powder Diffractometer at the Intense Pulsed Neutron Source (IPNS) at ANL. The TOF experiments are carried out at a fixed scattering angle, and diffraction patterns are generated as a function of incident neutron wavelength. Diffraction data are obtained at six separate detector banks, each positioned at a fixed angle relative to the incident beam. Since each detector bank views the sample from a different orientation, an assessment of preferred orientation (texture) in the sample can be obtained from variations in intensity from bank to bank. Reitveld refinements were carried out on the neutron diffraction data to obtain the lattice parameters and volume content of phases observed in the sample.

Microstructural analysis was conducted on samples polished through 1-μm diamond paste using a Zeiss 960A scanning electron microscope operating in both secondary and backscattered electron modes. Elemental compositions and spatial distributions were obtained with an Oxford energy dispersive spectrometer (EDS) and wavelength dispersive spectrometer (WDS) equipped with LINK_ISIS software.

3. Results and discussion

3.1. Neutron diffraction study

Peaks corresponding to five phases were identified in diffraction patterns of the SS–15Zr–2Tc alloy (see Fig. 1). These phases are the iron-based solid solutions ferrite and austenite, $ZrFe_2$-type Laves polytypes C36 and C15, and an $Fe_{23}Zr_6$-type intermetallic, the same as those observed in a SS–15Zr alloy without Tc [10]. Peaks corresponding to Tc-rich phases were not observed. Minor ZrO_{2-x} peaks present in the diffraction patterns were from the melt–crucible interaction residue on the SS–15Zr–2Tc alloy specimens and have not been included in our analyses.

The lattice parameters and amounts of phases in as-cast SS–15Zr and SS–15Zr–2Tc alloys are shown in Table 2. The lattice parameters of *all* phases are altered by Tc addition suggesting the incorporation of Tc into all phases of the alloy. The lattice parameters of ferrite and austenite are larger in the SS–15Zr–2Tc alloy than in the SS–15Zr alloy; this is to be expected since technetium is a larger atom than either Fe, Cr or Ni, the major components of the iron solid solution phases. The lattice parameters of the C36, C15, and $Fe_{23}Zr_6$-type intermetallic phases are smaller than the corresponding phases in the SS–15Zr alloy. The substitution of Tc at Zr sites of the intermetallic phases may explain the observed lattice contractions, since the atomic radius of Tc is smaller than that of Zr.

The amount of phases was calculated from Reitveld refinements on the neutron diffraction patterns. The

Table 1
Typical composition (wt%) of SS–15Zr–2Tc sample as measured by chemical analysis[a]

Fe	Cr	Ni	Zr	Mn	Mo	Si	Tc	O	N
Balance	13.7	10.9	14.5	1.2	1.7	0.5	1.7	0.04	0.02

[a] Uncertainty in measurement is ~10% of measured value.

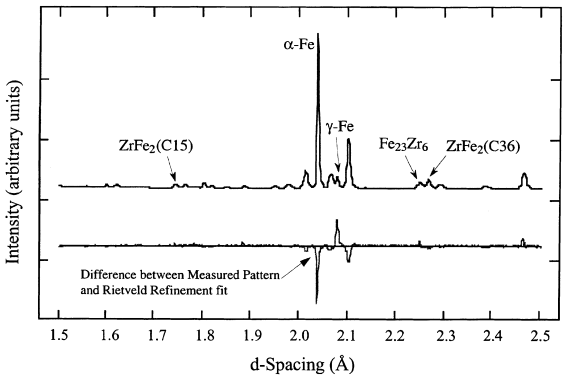

Fig. 1. Neutron Diffraction pattern from as-cast SS-15Zr–2Tc alloy. Prominent peaks from α-Fe (ferrite), γ-Fe (austenite), C36 and C15 Laves intermetallics, and the $Fe_{23}Zr_6$-type intermetallic are identified by arrows.

influence of texture on phase content has been minimized by averaging the results from all detector banks. The iron solid solution phase content in both SS–15Zr–2Tc and SS–15Zr alloys is ~50 vol.%; the ferrite and austenite content of the alloys are comparable. Significant differences are observed between the intermetallic phase contents of the alloys. The amounts of C15 and the $Fe_{23}Zr_6$-type phase are larger and the amount of C36 is smaller in SS–15Zr–2Tc than in the SS–15Zr alloy. Minor variations in casting conditions (such as cooling rate effects) may account for the observed differences. Alternatively, preferential dissolution of Tc into C15 and the $Fe_{23}Zr_6$-type phase may stabilize and increase the amount of these intermetallic phases.

3.2. Microstructural analysis

The typical microstructure in a SS–15Zr–2Tc alloy is shown in Fig. 2(a) and average phase compositions determined by point-to-point EDS analyses are shown in Table 3. The alloy microstructure is very similar to that in an alloy without Tc and shows ferrite (dark areas) and the Laves intermetallics (bright areas); austenite is observed along with the ferrite under appropriate contrast conditions (see Fig. 2(b)). Negligible quantities of zirconium are present in the ferrite and austenite; the element is present only in the intermetallic phases. Ferrite is prominent in the SS–15Zr–2Tc alloy microstructure, even though the alloying charge contains SS316, an austenitic stainless steel. The formation of ferrite in stainless steel-rich SS–Zr alloys has been discussed previously [11]. Nickel is very soluble in the Zr-based intermetallic phases; the depletion of nickel from the austenite results in austenite destabilization and the formation of ferrite.

The $ZrFe_2$-type Laves intermetallics C36 and C15 could not be differentiated by scanning electron microscopy; hence only one polytype composition is shown in Table 3. These intermetallics contained ~20 at.% Zr, a sub-stoichiometry of ~40% from the expected 33.3 at.% Zr. Similar sub-stoichiometry in these Laves intermetallics have been observed previously in Tc-free SS–15Zr alloys [11, 12]. The $Fe_{23}Zr_6$-type phase observed in the alloy is shown in Fig. 3; areas rich in zirconium were often observed within the phase. These zirconium-rich areas are believed to form during the transformation of the Laves intermetallics into the $Fe_{23}Zr_6$-type phase [10, 12].

The assessed Fe–Tc phase diagram [13] shows that pure iron has negligible solubility for technetium at room temperature. However, X-ray elemental maps obtained by WDS (Fig. 4) show that the element favors the iron solid solution phases over the intermetallic, with the highest enrichment occurring in the ferrite. The solubility of technetium in ferrite and austenite may be due to the presence of chromium and nickel in these iron solid solution phases. Both the assessed Cr–Tc phase diagram [14] and the Ni–Tc phase diagram [15] show large solubility for technetium at room temperature.

It is evident from Table 3 that technetium is present in all phases of the SS–15Zr–2Tc alloy. Since discrete Tc-rich phases are not observed, the release of the element will be governed by the corrosion behavior of the

Table 2
Lattice parameters and amount of phases in SS–15Zr[a] and SS–15Zr–2Tc alloys

Phases	Structure	Lattice parameters (nm)			Volume content (%)		
		SS–15Zr	SS–15Zr–2Tc	% Change	SS–15Zr	SS–15Zr–2Tc	Change
Ferrite	bcc	$a = 0.2876$	$a = 0.2879$	0.104	40 ± 6	44 ± 5	+4
Austenite	fcc	$a = 0.3596$	$a = 0.3598$	0.056	9 ± 1	7 ± 1	−2
$ZrFe_2$-type	Laves	$a = 0.4908$	$a = 0.4904$	−0.081	33 ± 5	19 ± 5	−14
	C36	$c = 1.6016$	$c = 1.5989$	−0.169			
$ZrFe_2$-type	Laves C15	$a = 0.6938$	$a = 0.6932$	−0.086	16 ± 2	22 ± 7	+6
$Fe_{23}Zr_6$-type	Th_6Mn_{23}-type	$a = 1.1690$	$a = 1.1660$	−0.257	2 ± 1	8 ± 1	+6

[a] Data from Ref. [10].

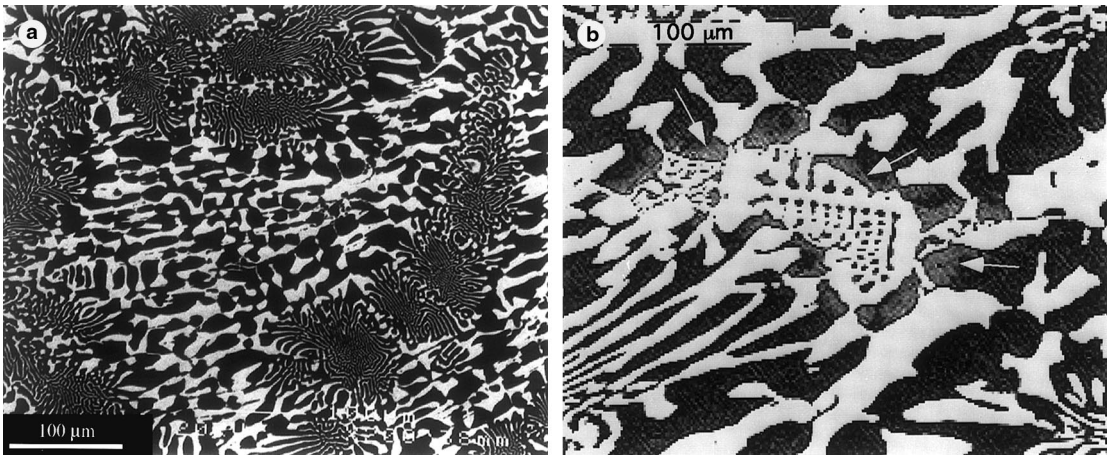

Fig. 2. (a) Typical microstructure in a SS–15Zr–2Tc alloy. The bright areas are the $ZrFe_2$-type Laves intermetallics; the dark areas contain ferrite and austenite. (b) Arrows indicate the austenite phase in a contrast-adjusted backscattered electron micrograph.

Table 3
Elemental compositions (at.%) determined by SEM/EDS analyses

	Fe	Cr	Ni	Zr	Mn	Mo	Si	Tc
Overall Alloy	57.1	16.6	12.4	8.6	1.5	0.9	1.1	1.1
Ferrite	66.2	23.5	5.3	Neg.[a]	1.6	1.2	0.4	1.6
Austenite	66.4	17.8	11.3	Neg.	1.9	0.7	0.6	1.3
$ZrFe_2$-type Intermetallic	45.4	5.7	23.9	20.2	1.6	0.7	1.4	1.0
$Fe_{23}Zr_6$-type Intermetallic	51.7	8.4	19.1	17.6	1.0	Neg.	1.3	0.9

[a] Negligible.

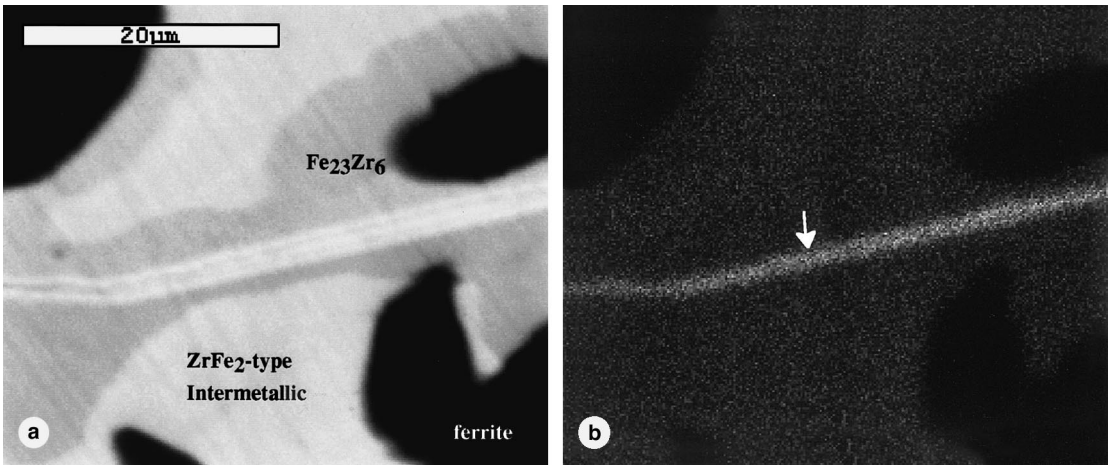

Fig. 3. (a) Backscattered electron image and (b) X-ray elemental map of Zr showing a narrow band of Zr-rich phase within the $Fe_{23}Zr_6$-type intermetallic.

main phases in the SS–15Zr waste form. Hence, we expect the corrosion behavior of Tc-containing SS–15Zr waste forms to be similar to the corrosion behavior of Tc-free SS–15Zr alloys, which have been described in other articles [3,16].

4. Conclusions

1. Technetium is incorporated in all phases of the SS–15Zr alloy; discrete Tc-rich phases were not observed in the alloy microstructure.

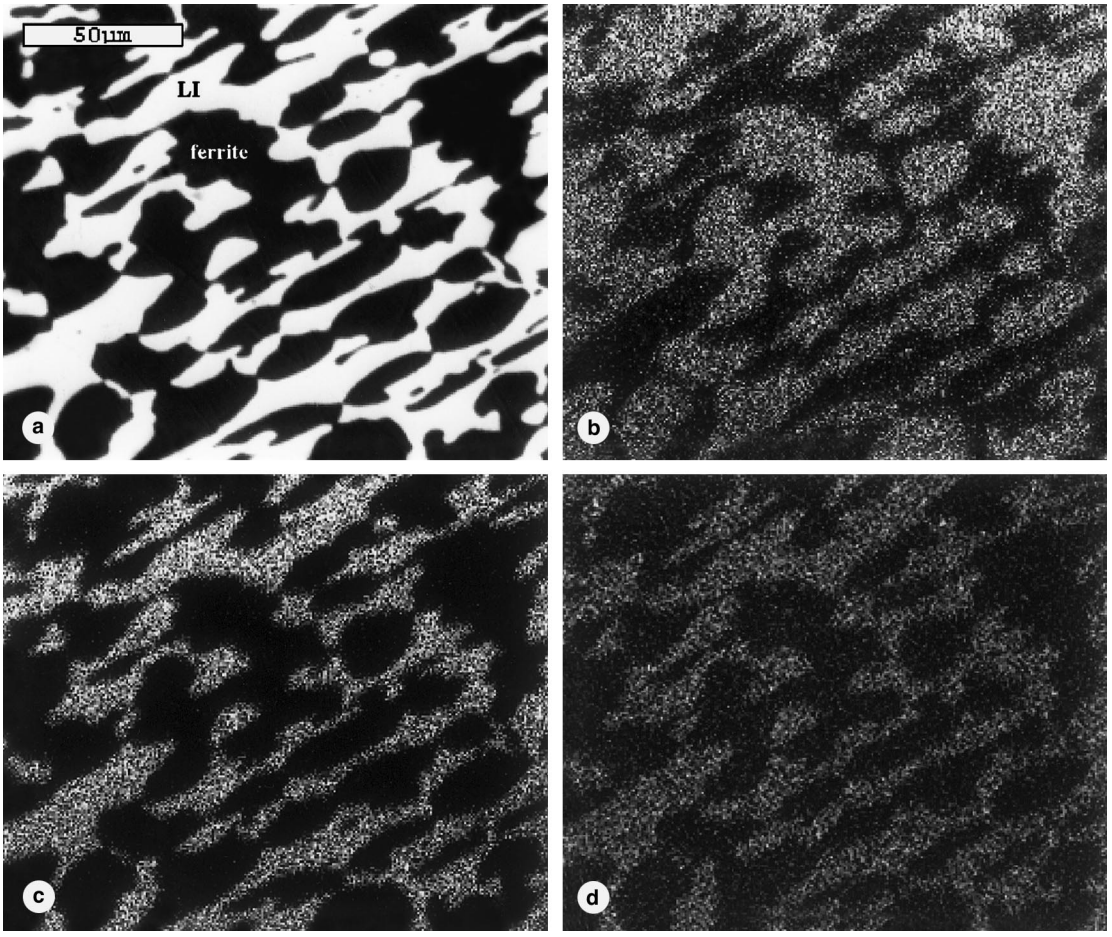

Fig. 4. (a) Backscattered electron image of SS–15Zr–2Tc alloy microstructure showing ferrite (dark) and Laves Intermetallics (bright). (b)–(d) are X-ray elemental maps showing the distribution of Tc, Zr and Ni in the alloy phases.

2. The lattice parameters of the $ZrFe_2$-type and $Fe_{23}Zr_6$-type intermetallics are smaller in a SS–15Zr alloy containing technetium; the element appears to substitute at the zirconium sites of the intermetallic lattice.
3. Technetium favors ferrite and austenite to the Zr-based intermetallics. The presence of chromium and nickel in the iron solid solution phases appears to have increased their solubility for technetium.

Acknowledgements

The support of the US Department of Energy, Reactor Systems, Development and Technology, under contract W-31-109-Eng-38 is recognized. This work has benefited from the use of the Intense Pulsed Neutron Source at Argonne National Laboratory. This facility is funded by the US Department of Energy, BES-Materials Science, under Contract No. W-31-109-ENG-38. We acknowledge the assistance of Steven Frank, Stephen Johnson, Dan Cummings and Tom O'Holleran, and thank Sean McDeavitt for helpful discussions.

References

[1] K. Schwochau, Radiochim. Acta 32 (1983) 139–152.
[2] J.P. Ackerman, T.R. Johnson, L.S.H. Chow, E.L. Carls, W.H. Hannum, J.J. Laidler, Prog. Nucl. Energy 31 (1997) 141.
[3] S.M. McDeavitt, D.P. Abraham, J.Y. Park, J. Nucl. Mater. 257 (1998) 21.
[4] K. Yoshihara, Topics in Current Chemistry, Springer, Berlin, vol. 176, 1996, pp. 17–35.
[5] J.G. Darab, P.A. Smith, Chem. Mater. 8 (1996) 1004.
[6] M.Y. Khalil, W.B. White, Mater. Res. Soc. Proc., 26, Elsevier, New York, 1984, pp. 655–662.

[7] D.J. Bradley, C.O. Harvey, R.P. Turcotte, Pacific Northwest Laboratory Report, PNL-3152, 1979.
[8] H. Lammertz, E. Merz, St. Halaszovich, Mater. Res. Soc. Proc., 44, Materials Research Society, PA, 1985, pp. 823–829.
[9] J. Vida, Dissertation, Institute for Hot Chemistry, Karlsruhe Nuclear Research Center, 1989.
[10] D.P. Abraham, J.W. Richardson Jr., S.M. McDeavitt, Mater. Sci. Eng. A239&240 (1997) 658.
[11] D.P. Abraham, S.M. McDeavitt, J.Y. Park, Metall. Mater. Trans. 27A (1996) 2151.
[12] D.P. Abraham, J.W. Richardson Jr., S.M. McDeavitt, Scripta Mat. 37 (1997) 239.
[13] H. Okamoto, in: T.P. Massalski (Ed.), Binary Alloy Phase Diagrams, vol. 2, ASM International, Materials Park, OH, 1990, p. 1780.
[14] M. Venkatraman, J.P. Neumann, in: T.P. Massalski (Ed.), Binary Alloy Phase Diagrams, vol. 2, ASM International, Materials Park, OH, 1990, p. 1342.
[15] P. Nash, in: T.P. Massalski (Ed.), Binary Alloy Phase Diagrams, vol. 2, ASM International, Materials Park, OH, 1990, p. 2870.
[16] D.P. Abraham, L.J. Simpson, M.J. DeVries, S.M. McDeavitt, Scientific Basis for Nuclear Waste Management XXII, Materials Research Society, Pittsburgh, PA, in press.